Deformation of Atomic $p_\pm$ Orbitals in Strong Elliptically Polarized Laser Fields: Ionization Time Drifts and Spatial Photoelectron Separation

Kunlong Liu,[1] Hongcheng Ni,[2,*] Klaus Renziehausen,[1] Jan-Michael Rost,[2,†] and Ingo Barth[1,‡]
[1]*Max-Planck-Institut für Mikrostrukturphysik, Weinberg 2, 06120 Halle (Saale), Germany*
[2]*Max-Planck-Institut für Physik komplexer Systeme, Nöthnitzer Strasse 38, 01187 Dresden, Germany*

(Received 20 June 2018; revised manuscript received 28 September 2018; published 15 November 2018)

We theoretically investigate the deformation of atomic $p_\pm$ orbitals driven by strong elliptically polarized (EP) laser fields and the role it plays in tunnel ionization. Our study reveals that different Stark effects induced by orthogonal components of the EP field give rise to subcycle rearrangement of the bound electron density, rendering the initial p_+ and p_- orbitals deformed and polarized along distinctively tilted angles with respect to the polarization ellipse of the EP field. As a consequence, the instantaneous tunneling rates change such that for few-cycle EP laser pulses the bound electron initially counterrotating (corotating) with the electric field is most likely released before (after) the peak of the electric field. We demonstrate that with a sequential-pulse setup one can exploit this effect to spatially separate the photoelectrons detached from p_+ and p_- orbitals, paving the way towards robust control of spin-resolved photoemission in laser-matter interactions.

DOI: 10.1103/PhysRevLett.121.203201

Understanding the response of bound electrons to strong fields leading eventually to ionization is a primary step towards controlling and interpreting attosecond dynamics of molecules [1–3], condensed-matter surfaces [4], and solids [5] driven by intense laser pulses. Tunneling ionization was recognized early in the 1960s as a key mechanism [6,7] and has been studied continuously ever since [8–12] due to its complicated nature and ever more refined experiments. Noble gases have been used mostly as convenient experimental systems to study the strong-field tunneling process [13–17]. Most observations had been interpreted based on the assumption of valence s orbitals [18], although the noble gases, apart from helium, naturally carry valence $p_\pm$ orbitals. Their ionization rates, however, are different in rotating fields due to nonadiabatic effects [10–12]. Recent experiments [19–21], which have observed the spin polarization of photoelectrons from noble gases driven by circularly polarized (CP) laser pulses, suggest that it is important and necessary to take into account distinct tunneling dynamics of the orbitals carrying opposite angular momenta in rotating fields [22–30].

In tunneling ionization of atoms so far studied, the bound electron is released with highest probability at the peaks of the oscillating laser field. This was predicted by theory [8,9] and verified in the experimental or numerical studies for valence p orbitals driven by linearly polarized laser pulses [31] and for s orbitals driven by elliptically polarized (EP) [32] or CP [33–37] pulses. Does this also hold for p orbitals exposed to strong EP laser pulses? Since most rare gas atoms have valence electrons of p character, this is a relevant question which we will address in the following by investigating theoretically the individual response of atomic $p_\pm$ orbitals to strong EP laser fields.

We start with the initial wave function for the p_+ orbital given by $\Psi_+^0(\mathbf{r}) = [\Psi_x(\mathbf{r}) + i\Psi_y(\mathbf{r})]/\sqrt{2}$, with the orthogonal normalized eigenfunctions $\Psi_x(\mathbf{r})$ and $\Psi_y(\mathbf{r})$. During the interaction with the laser field, the time-dependent wave function of the ground state can be written as $\Psi_+^0(\mathbf{r},t) = [b_x(t)\Psi_x(\mathbf{r}) + ib_y(t)\Psi_y(\mathbf{r})]e^{-iE_0 t}$, where E_0 is the binding energy and $b_j(t)$ (j denotes x or y) is the complex amplitude having the form $b_j(t) = b_{j,0}e^{-i\int_{-\infty}^{t}\delta H_j(t')dt'}$, with $b_{j,0} = 1/\sqrt{2}$. The term $\delta H_j(t)$ induced by the external field is a complex number [38], due to the coupling to excited and continuum states. Defining $\delta H_j(t) \coloneqq \delta E_j(t) + i\gamma_j(t)/2$, where $\delta E_j(t), \gamma_j(t) \in \mathbb{R}$, we can rewrite $\Psi_+^0(\mathbf{r},t)$ as

$$\Psi_+^0(\mathbf{r},t) = \frac{1}{\sqrt{2}}e^{\Gamma_x(t)}\Psi_x(\mathbf{r})e^{-i[E_0 t+\Phi_x(t)]} + \frac{1}{\sqrt{2}}e^{\Gamma_y(t)}\Psi_y(\mathbf{r})e^{-i[E_0 t+\Phi_y(t)]}e^{+i\frac{\pi}{2}}, \quad (1)$$

with $\Gamma_j(t) = \frac{1}{2}\int_{-\infty}^{t}\gamma_j(t')dt'$ and $\Phi_j(t) = \int_{-\infty}^{t}\delta E_j(t')dt'$. Here, $\gamma_j(t)$ is the relative variation rate of the population $P_j(t) = \frac{1}{2}e^{2\Gamma_j(t)}$ of $\Psi_j(\mathbf{r})$, as $\dot{P}_j(t)/P_j(t) = \gamma_j(t)$. $\delta E_j(t)$ can be understood as the instantaneous energy shift in the external field, known as Stark shift. The integration of $\delta E_j(t)$ over time will introduce an additional phase $\Phi_j(t)$ to the bound state.

For EP laser fields, interestingly, the unequal electric components in the x and y directions lead to different Stark shifts of $|\Psi_{p_x}\rangle$ and $|\Psi_{p_y}\rangle$. Thus, a phase offset $\Delta\Phi(t) = \Phi_y(t) - \Phi_x(t) = \int_{-\infty}^{t}[\delta E_y(t') - \delta E_x(t')]dt'$ between these two states will be accumulated during the interaction. By analyzing the angular distribution $G_{\pm}^{0}(\varphi, t) = \int_0^\infty dr\, r^2 \int_0^\pi d\theta \sin\theta |\Psi_{\pm}^{0}(\mathbf{r}, t)|^2$ of the electron density evolving from the initial p_+ or p_- orbital, we found that the orbital shape is associated with the population ratio $\mathcal{R}_{\pm}(t) = P_y^{\pm}(t)/P_x^{\pm}(t)$ and the phase offset $\Delta\Phi_{\pm}(t)$ [39]. In particular, $G_{\pm}^{0}(\varphi, t)$ always has maxima located aside from the coordinate axes if $\Delta\Phi_{\pm}(t) \neq N\pi$, $N \in \mathbb{Z}$. Now that the phase offset keeps being accumulated, one can conclude that the initial ring-shaped $p_{\pm}$ orbitals would be deformed and polarized generally along tilted angles with respect to the polarization ellipse of the EP field.

To understand intuitively how initial $p_{\pm}$ orbitals are deformed while interacting with EP pulses, we need to numerically calculate the population ratios and phase offsets for the interactions, based on the full three-dimensional time-dependent Schrödinger equation (TDSE) or, simply, a three-level model including $|\Psi_{p_x}\rangle$, $|\Psi_{p_y}\rangle$, and the first excited state above them [28,39]. Here, the valence $2p_{\pm}$ orbitals of Ne are chosen as initial orbitals. By projecting the time-dependent wave function onto $|\Psi_{p_x}\rangle$ and $|\Psi_{p_y}\rangle$, one can obtain the corresponding complex amplitudes and then calculate $\mathcal{R}_{\pm}(t)$ and $\Delta\Phi_{\pm}(t)$. We define the counterclockwise EP field as $\mathbf{E}(t) = \mathcal{E} f(t)[\cos(\omega t + \phi)\mathbf{e}_x + \epsilon \sin(\omega t + \phi)\mathbf{e}_y]$, with $f(t) = \sin^2[\pi t/(nT)]$ for $0 \leq t \leq nT$ and, otherwise, $f(t) = 0$. Here, $\mathcal{E}$, ϵ, ω, ϕ, n, and $T = 2\pi/\omega$ are the field amplitude, ellipticity, angular frequency, carrier-envelope phase (CEP), number of laser cycles, and optical period, respectively. We define $\tau = t - nT/2$ as the time difference from the field maximum. The initial orbital possessing the magnetic quantum number $m = 1$ ($m = -1$) is equivalent to the corotating (counterrotating) orbital with respect to the rotation of the electric field (see Fig. 1).

A three-cycle, 800 nm EP pulse with $\phi = 0$, $\mathcal{E} = 0.12$ a.u., and $\epsilon = 0.7$ is applied for the results shown in Fig. 1. In the upper panels, we depict the time-dependent magnitude of the electric field, as well as the population ratios and the phase offsets for the initial $p_{\pm}$ orbitals. The discrepancy between the results obtained from 3D TDSE and the three-level model is mainly due to the coupling to continuum and other excited states involved in TDSE. For both methods, one can find that $\mathcal{R}_+$ and $\mathcal{R}_-$ oscillate around one but out of phase while $\Delta\Phi_+$ and $\Delta\Phi_-$ vary with time similarly. If we apply the approximate relations $\mathcal{R}_+(t) \approx \mathcal{R}_-^{-1}(t)$ and $\Delta\Phi_+(t) \approx \Delta\Phi_-(t)$, then $G_-^0(\varphi, t) \approx G_+^0(\varphi + \pi/2, t)$ for negligible depletion can be obtained [39]; i.e., the initial p_+ and p_- orbitals would be deformed and aligned approximately perpendicularly. It can be seen in the lower panels of Fig. 1, where we plot the orbital shapes given by $G_{\pm}^{0}(\varphi, t)$ [39] at $\tau_- = -0.14\,T$, $\tau_0 = 0$, and $\tau_+ = 0.16\,T$. In

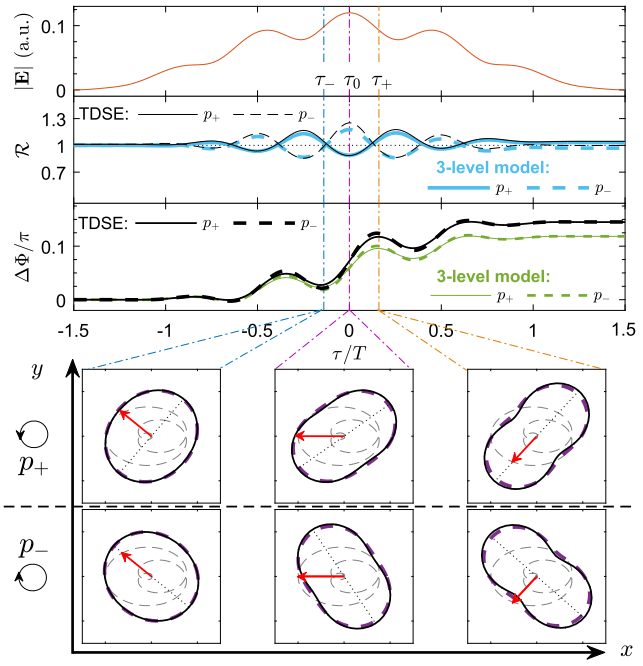

FIG. 1. Upper panels: The instantaneous magnitude of the electric field, the population ratio $\mathcal{R}$, and the phase offset $\Delta\Phi$ as functions of time. Lower panels: The orbital shapes (solid, TDSE; thick dashed, three-level model) at τ_-, τ_0, and τ_+. The alignments of the orbitals (dotted lines), the profile of the electric field (thin dashed curves), and the instantaneous field vectors (arrows) are shown inside the lower panels.

particular, at τ_- (τ_+), the alignment of the deformed p_- (p_+) orbital is parallel to the vector of the electric field. Then, the instantaneous ionization rate is expected to be a compromise between the instantaneous strength of the EP field and the tilted alignment of the orbital. According to the orbital deformations shown in Fig. 1, we anticipate that the highest ionization rate would appear *before* τ_0 (i.e., the field maximum) for the initial p_- orbital but *after* τ_0 for p_+.

Next, we aim to obtain a "semiadiabatic" formula for the instantaneous ionization rate for deforming orbitals, based on the Perelomov-Popov-Terent'ev (PPT) theory [7] for CP fields [10,11]. To this end, two assumptions are made. (I) The cycle-averaged ionization rate $w_{\pm}^{\mathrm{CP}}(\omega, \mathcal{E})$ given in the PPT theory [7] for $p_{\pm}$ orbitals in CP fields [10,11] is considered here as the *instantaneous* ionization rate, as the strength and the angular frequency of the infinite CP field are constant in time. (II) For EP fields within a limited time duration $(t - \delta t/2, t + \delta t/2)$, the rotational electric field is treated as a fraction of the CP field with the amplitude $\mathcal{E}_t = |\mathbf{E}(t)|$ and the angular frequency $\omega_t = \partial\theta_t/\partial t = \epsilon\omega[\mathcal{E} f(t)/\mathcal{E}_t]^2$, where θ_t is the angle of $\mathbf{E}(t)$. Our assumptions indicate that nonadiabatic effects from the field rotation are retained but that from the envelope variation is neglected since it would be less significant [36]. Then, the instantaneous ionization rate for *pure* $p_{\pm}$ orbitals in EP fields can be approximately given by $\mu_t^{\pm} \approx w_{\pm}^{\mathrm{CP}}(\omega_t, \mathcal{E}_t)$.

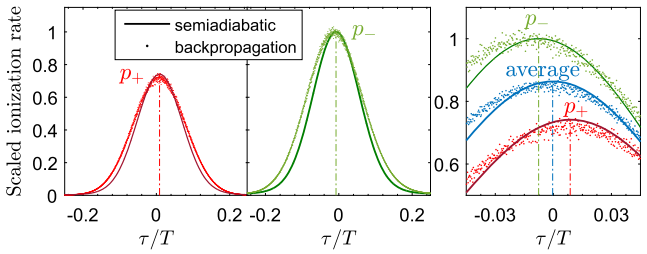

FIG. 2. Tunnel ionization rates for the interactions of the initial $p_\pm$ orbitals with the EP pulse given in Fig. 1. Their average is presented in the enlarged figure on the right-hand side. The results are obtained from the semiadiabatic formula Eq. (2) (solid curves) and backpropagation (dots), respectively. The vertical dash-dotted lines indicate the maxima of the semiadiabatic ionization rates. The rates have been scaled with respect to the maxima of those for p_-.

However, due to the orbital deformation induced by the Stark effect as described above, the instantaneous orbital is no longer a pure p_+ or p_- orbital but becomes a superposition of them. Therefore, the instantaneous ionization rate for the deforming orbital should be given in a coherent way [39]:

$$\mu_m^{\mathrm{EP}}(t) \sim |b_m^+(t)\sqrt{\mu_t^+}e^{i\theta_i} + b_m^-(t)\sqrt{\mu_t^-}e^{-i\theta_i}|^2. \quad (2)$$

Here, $b_m^\pm(t)$ are the complex amplitudes of the $|\Psi_{p_\pm}\rangle$ eigenstates and can be obtained from numerical calculations [39]. The subscript $m = \pm 1$ denotes the initial $p_\pm$ orbitals. The terms $e^{i\theta_i}$ and $e^{-i\theta_i}$ account, respectively, for the local phases of the p_+ and p_- orbitals at the emitting angle $\theta_i = \theta_t + \pi$ of the ionizing wave packets.

For initial $p_\pm$ orbitals driven by the EP pulse given in Fig. 1, the instantaneous ionization rates obtained from the semiadiabatic formula are depicted in Fig. 2. It shows that not only the ionization rates but also the times for the highest ionization rates are sensitive to the initial rotation of the bound electron. For the p_- orbital, the ionization peak is drifted to an earlier time, whereas the one for p_+ is delayed, with respect to the field maximum. For verification, we apply the backpropagation method [34–36] in our TDSE simulations [39] to obtain the time-dependent ionization rates, which are also shown in Fig. 2. It can be seen that the ionization rates and the peak drifts in time given by the semiadiabatic formula agree qualitatively with those obtained from numerical calculations.

From the experimental viewpoint, the ionization time drifts can be demonstrated by the attoclock setup [32,33]. We show in Figs. 3(a) and 3(b) the photoelectron angular distributions (PADs) obtained from TDSE for the interactions of $p_\pm$ orbitals with the EP pulse. For comparison, the results for the CP pulse and otherwise the same pulse parameters are shown in Figs. 3(d) and 3(e). The differences between the normalized photoelectron momentum distributions (PMDs) (integrated over k_z) for initial p_+

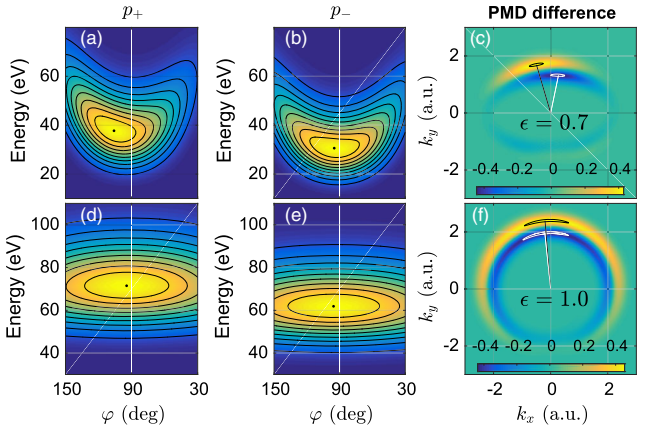

FIG. 3. The PADs for the p_+ [(a),(d)] and p_- [(b),(e)] orbitals and the differences [(c),(f)] between the normalized PMDs for the $p_\pm$ orbitals, under the EP (upper row) and CP (lower row) pulses, respectively. The colors are in linear scales. The PADs are normalized to their maxima and the step of the contour is 0.1. The black and white contours in (c) and (f) indicate 97% of the maxima and minima, respectively.

and p_- orbitals are shown in Figs. 3(c) and 3(f). In general, the photoelectron from the initial p_+ orbital has a higher kinetic energy than that from p_-, due to their different initial transverse momenta [12,39]. For the EP pulse, however, the faster electron that experiences smaller Coulomb effect ends up with a larger deflected angle. It suggests that the electron initially in the p_+ orbital is released at a delayed time compared to that for p_-, according to the attoclock configuration [32,33].

In Fig. 4(a), we depict the offset angles extracted from the PADs for initial $p_\pm$ orbitals (integrated over the kinetic energy) as a function of the pulse ellipticity. Those extracted from the averaged PADs are also presented, while

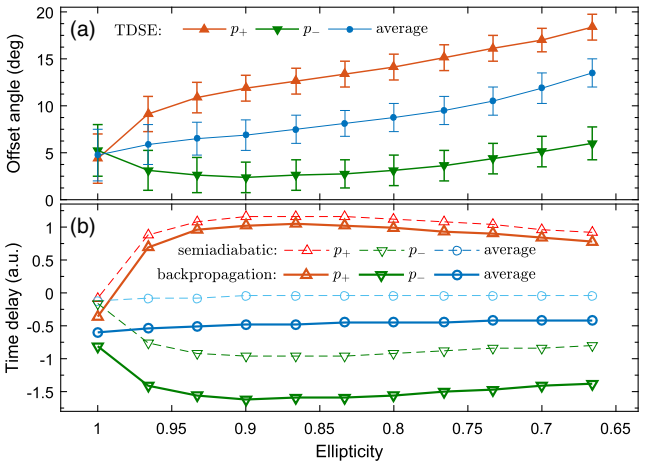

FIG. 4. The ellipticity dependence of (a) the offset angles (deviation from $\varphi = 90°$) of the PADs and (b) the delay of the highest ionization rate with respect to the field maximum. The error bar in (a) indicates the range for the yield higher than 99.95% of the peak value.

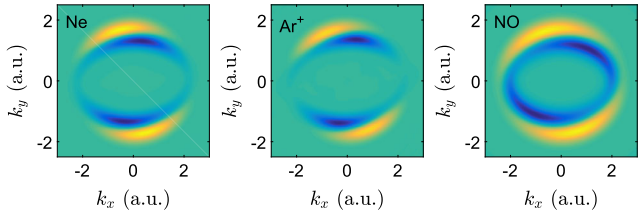

FIG. 5. The differences between the CEP-averaged, normalized PMDs for the valence current-carrying orbitals of Ne, Ar^+, and NO. Calculation details are shown in Ref. [39]. Other laser parameters are the same as in Fig. 1.

the p_0 orbital has hardly any contribution. One can see that once the ellipticity decreases from one, the offset angle for p_+ increases significantly compared to that of the average PAD, pointing to a positive delay of the ionization time. Meanwhile, for p_- the offset angle exhibits a decreasing tendency at first and then increases gradually, and it is smaller than that of the average PAD. It demonstrates that the ionization for p_- takes place with highest probability before the field maximum. Note that as the ellipticity further decreases, the Coulomb effect on the photoelectron is enhanced and, thus, the increasing momentum drift caused by the Coulomb potential leads to the increasing offset angle even for the negative ionization time delay.

Applying the semiadiabatic formula and the backpropagation method based on TDSE, we further study the ellipticity dependence of the time delay for the highest ionization rate. The results shown in Fig. 4(b) reveal that the drifts of the ionization times for p_+ and p_- are opposite to each other for EP pulses, in contrast to those for CP pulses [29,30]. When the ellipticity further decreases, the pulse tends to be linearly polarized and the orbital deformation no longer plays a role in altering the ionization time. Thus, after passing the extrema the ionization time drifts tend to be reduced with decreasing ellipticity. Note that the discrepancy between the outcomes of the two methods is likely due to the influence of the excited states [23,42] involved in TDSE.

The differences between the CEP-averaged, normalized PMDs for the valence $p_\pm$ orbitals of Ne and Ar^+ and $\pi_\pm$ orbitals for prealigned nitric oxide (NO) are presented in Fig. 5, respectively. Despite systematical discrepancies such as ionization potentials and Coulomb effect, it is shown that the faster photoelectrons from initially corotating orbitals are always deflected more. Such phenomenon has been observed in experiments via preparing the ring-current states of Ar^+ [43]. So far, the orbital deformation in EP laser fields and the consequent ionization time drift appear to be universal for current-carrying orbitals of atoms and molecules.

An appealing consequence of the asymmetric ionization dynamics for valence $p_\pm$ orbitals is the spin polarization of photoelectrons from rare gases, which was recently observed with respect to the photoelectron kinetic energy [19–21]. Based on the orbital deformation mechanism revealed by the present study, we demonstrate below a novel scheme to *spatially* separate the photoelectrons removed from p_+ and p_- orbitals. Our idea is to decompose the EP pulse into a linearly polarized (LP) pulse and a CP pulse. According to the analysis above, the former component is essentially the origin of the phase offset and, thus, the deformation of current-carrying orbitals. Thereby, we propose to apply a weak and long LP pulse to steer the orbital deformation and a subsequent strong CP pulse to trigger the photoemission, as shown in Fig. 6(a).

We have numerically solved the 3D TDSE for the interactions between $p_\pm$ orbitals of Ne and two sequential 800-nm pulses (a 30-cycle LP pulse and a three-cycle CP pulse). Figure 6(b) shows the total PMDs $Y(k_x, k_y) = Y_+(k_x, k_y) + Y_-(k_x, k_y)$ (integrated over k_z) for $p_\pm$ orbitals driven by a single CP pulse and by the sequential LP and CP pulses. The surface color indicates the PMD asymmetry $[Y_+(k_x, k_y) - Y_-(k_x, k_y)]/Y(k_x, k_y)$. One can see that the weak LP pulse hardly affects the total yield but significantly modifies the momentum distributions of photoelectrons from $p_\pm$ orbitals. In particular, after adding the LP pulse, the asymmetry reaches nearly $\pm 100\%$ and, meanwhile, the local ionization yields for large asymmetry are remarkably enhanced, in contrast to the case with one single CP pulse. This will potentially enable us to produce highly spin-polarized photoelectrons with considerable yield from rare gases [22] or nitric oxide [23–25]. In addition, we show in Fig. 6(c) the PADs for

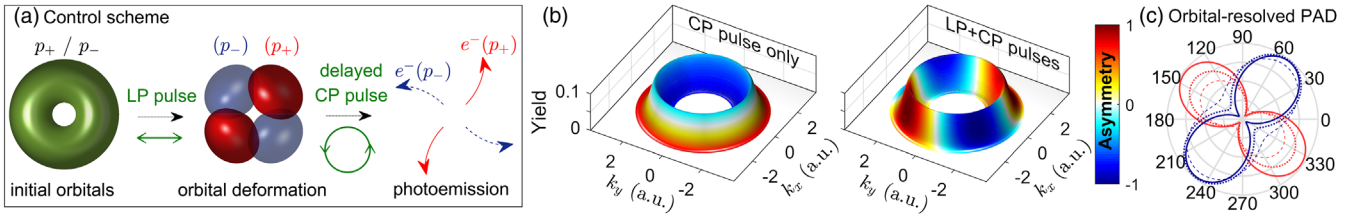

FIG. 6. (a) Control scheme to spatially separate photoelectrons removed from valence current-carrying orbitals. (b) The total PMDs with the surface color indicating the PMD asymmetry of $p_\pm$ orbitals. The intensities for the LP and CP pulses are 9.5×10^{13} and 1.0×10^{15} W/cm^2, respectively. (c) The PADs for p_+ (red) and p_- (blue) orbitals within the sequential-pulse scheme using the LP pulse with different intensities: 3.6×10^{13} W/cm^2 (dashed), 6.2×10^{13} W/cm^2 (dotted), and 9.5×10^{13} W/cm^2 (solid). All results have been averaged over the CEP of the CP pulse.

initial $p_{\pm}$ orbitals within our scheme using different intensities for the LP pulse. It suggests that the orbital-resolved PADs and thus the PMD asymmetry can be optimized via simply adjusting the intensity of the LP pulse.

In this Letter, we have demonstrated that current-carrying orbitals are deformed by strong EP fields, resulting in the modification of instantaneous ionization rates. In contrast to the prevalent tunneling picture, the bound electron is released with highest probability before or after the peak of the EP field, depending on the sign of the magnetic quantum number of the initial current-carrying orbital. For the future, our study suggests that tailored intense fields [44,45] with different electric components in two orthogonal directions could also lead to orbital deformations and alter the most probable ionization times for current-carrying orbitals. Furthermore, we have proposed a sequential-pulse scheme for the spatial separation of photoelectrons removed from valence $p_{\pm}$ orbitals. By considering the spin-orbit coupling [22,23], the sensitivity of the most probable ionization times to the sense of initial electron rotation in tailored intense laser fields will open the prospect of manipulating the separation of spin-up and spin-down photoelectrons from atoms [19–22], molecules [23–25], and, potentially, solids.

K. L. and I. B. thank R. Dörner, O. Smirnova, and M. Ivanov for stimulating discussions. Financial support from the Max Planck Society for the Max Planck Research Group "Current-Carrying Quantum Dynamics" (CCQD), the Deutsche Forschungsgemeinschaft, Priority Programme 1840 "Quantum Dynamics in Tailored Intense Fields" (QUTIF), and the Alexander von Humboldt-Stiftung is acknowledged.

*Present address: Institute of Theoretical Physics, Technische Universität Wien, Wiedner Hauptstrasse 8-10/136, 1040 Vienna, Austria.
nih@pks.mpg.de
†rost@pks.mpg.de
‡barth@mpi-halle.mpg.de

[1] X. M. Tong, Z. X. Zhao, and C. D. Lin, Phys. Rev. A **66**, 033402 (2002).
[2] B. Wolter, M. G. Pullen, A.-T. Le, M. Baudisch, K. Doblhoff-Dier, A. Senftleben, M. Hemmer, C. D. Schröter, J. Ullrich, T. Pfeifer, R. Moshammer, S. Gräfe, O. Vendrell, C. D. Lin, and J. Biegert, Science **354**, 308 (2016).
[3] K. Liu and I. Barth, Phys. Rev. Lett. **119**, 243204 (2017).
[4] A. L. Cavalieri, N. Müller, Th. Uphues, V. S. Yakovlev, A. Baltuška, B. Horvath, B. Schmidt, L. Blümel, R. Holzwarth, S. Hendel, M. Drescher, U. Kleineberg, P. M. Echenique, R. Kienberger, F. Krausz, and U. Heinzmann, Nature (London) **449**, 1029 (2007).
[5] G. Ndabashimiye, S. Ghimire, M. Wu, D. A. Browne, K. J. Schafer, M. B. Gaarde, and D. A. Reis, Nature (London) **534**, 520 (2016).
[6] L. V. Keldysh, Sov. Phys. JETP **20**, 1307 (1965).
[7] A. M. Perelomov, V. S. Popov, and M. V. Terent'ev, Sov. Phys. JETP **23**, 924 (1966); **24**, 207 (1967); A. M. Perelomov and V. S. Popov, Sov. Phys. JETP **25**, 336 (1967).
[8] G. L. Yudin and M. Y. Ivanov, Phys. Rev. A **64**, 013409 (2001).
[9] L. Torlina and O. Smirnova, Phys. Rev. A **86**, 043408 (2012); **86**, 043409 (2012).
[10] I. Barth and O. Smirnova, Phys. Rev. A **84**, 063415 (2011); **85**, 029906(E) (2012); **85**, 039903(E) (2012).
[11] I. Barth and O. Smirnova, Phys. Rev. A **87**, 013433 (2013).
[12] J. Kaushal, F. Morales, and O. Smirnova, Phys. Rev. A **92**, 063405 (2015).
[13] D. Shafir, H. Soifer, C. Vozzi, A. S. Johnson, A. Hartung, Z. Dube, D. M. Villeneuve, P. B. Corkum, N. Dudovich, and A. Staudte, Phys. Rev. Lett. **111**, 023005 (2013).
[14] M. Li, Y. Liu, H. Liu, Q. Ning, L. Fu, J. Liu, Y. Deng, C. Wu, L. Y. Peng, and Q. Gong, Phys. Rev. Lett. **111**, 023006 (2013).
[15] N. Camus, E. Yakaboylu, L. Fechner, M. Klaiber, M. Laux, Y. Mi, K. Z. Hatsagortsyan, T. Pfeifer, C. H. Keitel, and R. Moshammer, Phys. Rev. Lett. **119**, 023201 (2017).
[16] Y. L. Wang, S. G. Yu, X. Y. Lai, X. J. Liu, and J. Chen, Phys. Rev. A **95**, 063406 (2017).
[17] X. Gong, C. Lin, F. He, Q. Song, K. Lin, Q. Ji, W. Zhang, J. Ma, P. Lu, Y. Liu, H. Zeng, W. Yang, and J. Wu, Phys. Rev. Lett. **118**, 143203 (2017).
[18] H. Xie, M. Li, S. Luo, Y. Li, Y. Zhou, W. Cao, and P. Lu, Phys. Rev. A **96**, 063421 (2017).
[19] A. Hartung, F. Morales, M. Kunitski, K. Henrichs, A. Laucke, M. Richter, T. Jahnke, A. Kalinin, M. Schöffler, L. P. H. Schmidt, M. Ivanov, O. Smirnova, and R. Dörner, Nat. Photonics **10**, 526 (2016).
[20] M.-M. Liu, Y. Shao, M. Han, P. Ge, Y. Deng, C. Wu, Q. Gong, and Y. Liu, Phys. Rev. Lett. **120**, 043201 (2018).
[21] D. Trabert, A. Hartung, S. Eckart, F. Trinter, A. Kalinin, M. Schöffler, L. P. H. Schmidt, T. Jahnke, M. Kunitski, and R. Dörner, Phys. Rev. Lett. **120**, 043202 (2018).
[22] I. Barth and O. Smirnova, Phys. Rev. A **88**, 013401 (2013).
[23] K. Liu and I. Barth, Phys. Rev. A **94**, 043402 (2016).
[24] K. Liu, K. Renziehausen, and I. Barth, Phys. Rev. A **95**, 063410 (2017).
[25] K. Liu and I. Barth, J. Mod. Opt. **64**, 987 (2017).
[26] D. B. Milošević, Phys. Rev. A **93**, 051402(R) (2016).
[27] T. Herath, L. Yan, S. K. Lee, and W. Li, Phys. Rev. Lett. **109**, 043004 (2012).
[28] I. Barth and M. Lein, J. Phys. B **47**, 204016 (2014).
[29] J. P. Wang and F. He, Phys. Rev. A **95**, 043420 (2017).
[30] Q. Zhang, G. Basnayake, A. Winney, Y. F. Lin, D. Debrah, S. K. Lee, and W. Li, Phys. Rev. A **96**, 023422 (2017).
[31] M. Uiberacker, T. Uphues, M. Schultze, A. J. Verhoef, V. Yakovlev, M. F. Kling, J. Rauschenberger, N. M. Kabachnik, H. Schröder, M. Lezius, K. L. Kompa, H. G. Muller, M. J. J. Vrakking, S. Hendel, U. Kleinegerg, U. Heinzmann, M. Drescher, and F. Krausz, Nature (London) **446**, 627 (2007).
[32] P. Eckle, A. N. Pfeiffer, C. Cirelli, A. Staudte, R. Dörner, H. G. Muller, M. Büttiker, and U. Keller, Science **322**, 1525 (2008).

[33] L. Torlina, F. Morales, J. Kaushal, I. Ivanov, A. Kheifets, A. Zielinski, A. Scrinzi, H. G. Muller, S. Sukiasyan, M. Ivanov, and O. Smirnova, Nat. Phys. **11**, 503 (2015).
[34] H. Ni, U. Saalmann, and J.-M. Rost, Phys. Rev. Lett. **117**, 023002 (2016).
[35] H. Ni, U. Saalmann, and J.-M. Rost, Phys. Rev. A **97**, 013426 (2018).
[36] H. Ni, N. Eicke, C. Ruiz, J. Cai, F. Oppermann, N. I. Shvetsov-Shilovski, and L.-W. Pi, Phys. Rev. A **98**, 013411 (2018).
[37] N. Eicke and M. Lein, Phys. Rev. A **97**, 031402 (2018).
[38] M. Chini, B. Zhao, H. Wang, Y. Cheng, S. X. Hu, and Z. Chang, Phys. Rev. Lett. **109**, 073601 (2012).
[39] See Supplemental Material at http://link.aps.org/supplemental/10.1103/PhysRevLett.121.203201 for the details of the theoretical derivations, the numerical calculations, the semiadiabatic fomula, and the backpropagation method, which includes Refs. [40,41].
[40] M. D. Feit, J. A. Fleck, Jr., and A. Steiger, J. Comput. Phys. **47**, 412 (1982).
[41] X. M. Tong, K. Hino, and N. Toshima, Phys. Rev. A **74**, 031405(R) (2006).
[42] M. Sabbar, H. Timmers, Y.-J. Chen, A. K. Pymer, Z.-H. Loh, S. G. Sayres, S. Pabst, R. Santra, and S. R. Leone, Nat. Phys. **13**, 472 (2017).
[43] S. Eckart, M. Kunitski, M. Richter, A. Hartung, J. Rist, F. Trinter, K. Fehre, N. Schlott, K. Henrichs, L. P. H. Schmidt, T. Jahnke, M. Schöffler, K. Liu, I. Barth, J. Kaushal, F. Morales, M. Ivanov, O. Smirnova, and R. Dörner, Nat. Phys. **14**, 701 (2018).
[44] A. Fleischer, O. Kfir, T. Diskin, P. Sidorenko, and O. Cohen, Nat. Photonics **8**, 543 (2014).
[45] X. Gong, C. Lin, F. He, Q. Song, K. Lin, Q. Ji, W. Zhang, J. Ma, P. Lu, Y. Liu, H. Zeng, W. Yang, and J. Wu, Phys. Rev. Lett. **118**, 143203 (2017).